JGR Atmospheres

RESEARCH ARTICLE
10.1029/2020JD033465

Special Section:
Years of the Maritime Continent

Systematic Patterns in Land Precipitation Due to Convection in Neighboring Islands in the Maritime Continent During MJO Propagation

Haochen Tan[1], Pallav Ray[1], Bradford Barrett[2], Jimy Dudhia[3], and Mitchell W. Moncrieff[3]

[1]Meteorology, Ocean Engineering and Marine Sciences, Florida Institute of Technology, Melbourne, FL, USA, [2]Oceanography Department, US Naval Academy, Annapolis, MD, USA, [3]Mesoscale & Microscale Meteorology Lab, National Center for Atmospheric Research, Boulder, CO, USA

Key Points:

- Precipitation increases over islands that are located to the east of removed island during MJO propagation under background westerlies
- Stronger westerlies aided by Coriolis lead to an increase in vertical advection of moisture over an island to the east of the removed island
- During lower-tropospheric easterlies, no systematic pattern of rainfall variation is found to the east of the removed islands

Correspondence to:
H. Tan,
htan2013@my.fit.edu

Citation:
Tan, H., Ray, P., Barrett, B., Dudhia, J., & Moncrieff, M. W. (2021). Systematic patterns in land precipitation due to convection in neighboring islands in the Maritime Continent during MJO propagation. *Journal of Geophysical Research: Atmospheres*, *126*, e2020JD033465. https://doi.org/10.1029/2020JD033465

Received 6 JUL 2020
Accepted 12 JAN 2021

Abstract The land-sea contrast in the Maritime Continent (MC) has been found to influence the Madden–Julian Oscillation (MJO). However, the specific contribution from individual islands to the precipitation over the surrounding islands during MJO propagation is not well known. We found that when an island is removed in the presence of lower-tropospheric westerlies, precipitation increases over islands that are located to its east due to the strengthening of the westerlies. Frictional convergence of the stronger westerlies, aided by Coriolis, leads to an increase in vertical advection of moisture and precipitation over an island located to the east. On the other hand, the reduced heating over the removed island reduces the westerlies and precipitation to the west of the removed island and is consistent with the response of large-scale circulation to tropical heating. During background easterlies prior to MJO arrival, a systematic decrease in precipitation was found in the surrounding islands to the west side of the removed island. But, on the eastern side of the removed island, no systematic change in precipitation was found. The results imply that changes in large-scale circulation in response to convection (or a lack thereof) over a removed island may significantly influence precipitation in the neighboring islands. Therefore, biases in model precipitation over an island in the MC may arise from bias in precipitation over a neighboring island. Moreover, the presence of different island chains in the MC has led to a more conducive environment for more overall precipitation over the islands in the MC.

Plain Language Summary The Maritime Continent (MC) with its islands and seas receives a large amount of precipitation and influences the global weather and climate. Therefore, understanding the spatial distribution of precipitation in the MC is important, in particular, during the times of enhanced convection. One such period of enhanced convection is associated with the Madden–Julian Oscillation (MJO) as it propagates over the MC from west to east with a period of 20–100 days. In this study, the specific role of individual islands in modulating rainfall on other islands during the MJO propagation is explored using regional model simulations. We found a systematic pattern in change in rainfall during the westerly phase of MJO propagation.

1. Introduction

As the largest archipelago in the world, the Maritime Continent (MC) plays a significant role in modulating the modes of large-scale, atmospheric intraseasonal variability, such as the Madden–Julian Oscillation (MJO, Madden & Julian, 1971, 1972; Zhang, 2005). The MC features a unique, complex system of mountainous islands, narrow peninsulas, and shallow seas (Ramage, 1968). The land-sea contrast and topography in the MC (Figure 1a) have been found to influence the amplitude and propagation of the MJO (Ahn et al., 2020; Ajayamohan et al., 2013; S. M. Hagos et al., 2016; H. H. Hsu & Lee, 2005; Ray et al., 2011; Sobel et al., 2010; Tan et al., 2020; Tseng et al., 2017; Wu & Hsu, 2009). Inness and Slingo (2006) demonstrated that when the MJO crosses the MC, it may split into two parts: one moving northward and the other moving southward. Half of the MJO events are able to cross the MC (Kerns & Chen, 2020), about 25% cross the MC without weakening (Zhang & Ling, 2017), and the rest of the events are disrupted or completely diminished (Feng et al., 2015; Kim et al., 2014). The MC landmass can also limit air–sea interaction, creating zonal land-sea gradients of surface latent heat flux that slow the eastward propagation of the MJO (Tseng et al., 2015).

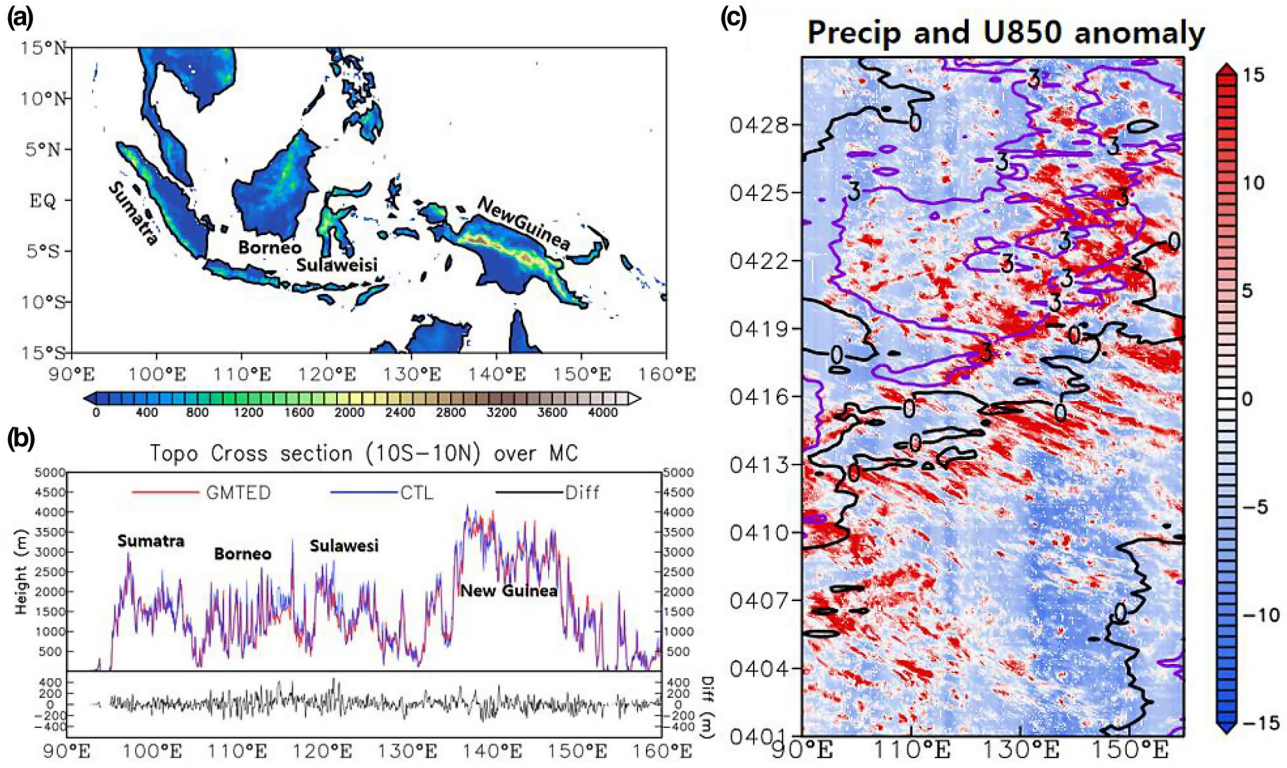

Figure 1. (a) Topography (in m), (b) cross section of maximum topography height over 10°S–10°N from global multiresolution terrain elevation (GMTED, red line), model (blue line), and difference (CTL minus GMTED, black line), and (c) time–longitude diagrams of positive daily anomalies of zonal winds at 850 hPa (U850, contour levels in 0 and 3 m s^{-1}) from the ERA-Interim, and precipitation (shaded, mm day^{-1}) from the CMORPH, both averaged over 10°S–10°N.

Previous studies have also demonstrated that forcing from upstream is important for triggering new convection associated with the MJO (e.g., Lau & Peng, 1987; Matthews, 2008; Seo & Kim, 2003). Others have explored the land-sea breeze and mountain breeze circulations (e.g., Qian, 2007, 2019; Simpson et al., 1993; Yang & Slingo, 2001) in response to land convection. Despite the known influence of land-sea contrast, topography, and the competition for moisture and convection among different islands in the MC (e.g., Birch et al., 2016; Peatman et al., 2014; Qian, 2007; Rauniyar & Walsh, 2011), few studies have explored the role of an individual island group in the MC on the precipitation over the surrounding islands during MJO propagation. In this study, we examine the role of land convection on large-scale circulation and how this change in circulation may impact precipitation over neighboring islands. We specifically focus on periods with lower-tropospheric westerly winds in the MC that are commonly associated with MJO propagation (e.g., Moum et al., 2014).

There are two main motivations behind this study: (1) to understand the variability of MJO-related precipitation, and (2) to understand the distribution of climatological precipitation in the MC due to the presence of individual islands. These two aspects, however, are not independent of each other. Specifically, recent work by Kerns and Chen (2020) suggested that the MJO contributes about 40%–50% of the annual precipitation over the tropical Indo-Pacific warm pool. Therefore, MJO-related precipitation variability is expected to affect the mean precipitation in the MC. On the other hand, the role of the mean state on MJO variability is well established (e.g., Zhang & Dong, 2004). The rest of the paper is organized as follows: model, data, and methods are discussed in Section 2, followed by results in Section 3, and a summary in Section 4.

2. Model and Data

The MJO in this study is analyzed using the Weather Research and Forecasting Model version 3.8.1 (WRF; Skamarock et al., 2008), a fully compressible, terrain-following model. The simulations are conducted with a one-way nested configuration. The simulations have 41 sigma levels with 9 levels in the lowest 1 km, and the model top is at 10 hPa. The integration time step for all simulations is 60 s. The model output is saved every hour. The horizontal grid-spacing of the model is 12 km and has 794 × 363 horizontal points, which covers the entire MC (80°–160°E, 20°S–20°N). The topography and land use data are from the global multiresolution terrain elevation (GMTED2010, 30 arc-second, Danielson & Gesch, 2011) data set (see Figure 1b).

We use the following parameterization schemes for the simulations: the Kain–Fritsch (Kain et al., 2004) scheme for the cumulus parameterization; Noah land surface model (Chen & Dudhia, 2001) for the surface layer parameterization; the Rapid Radiative Transfer Model (RRTMG, Iacono et al., 2008) scheme for longwave radiation; the updated Goddard scheme (Chou & Suarez, 1994; Shi et al., 2010) for shortwave radiation; the Mellor–Yamada–Janjić (Janjić, 1994) scheme for the planetary boundary layer; and the WRF Single Moment 6 (WSM6, Lim & Hong, 2010) scheme for microphysics. Further details on the model configuration can be found in Tan et al. (2020).

To quantify the role of land-sea contrast of the individual islands, four experiments are conducted: a control simulation (CTL) with realistic topography (see Figure 1b) that serves as a benchmark to be compared with the sensitivity experiments, and three sensitivity experiments that involve the land removal (and replacement with water) of Sumatra and Java (E1L), Borneo and Sulawesi (E2L), and New Guinea (E3L) Islands. The sea surface temperatures (SSTs) for the removed islands were generated by interpolating from nearby oceanic grid points to fill the space previously occupied by land. The differences in precipitation between the land-removal experiments and the CTL simulation are interpreted as estimates of the influence of each removed island group. The initial and lateral boundary conditions, along with the SST, are based on the ERA-Interim (Dee et al., 2011; 6-hourly) reanalysis. The results using constant SST (i.e., SST fixed at the model initial time) were similar to that in CTL simulation (not shown).

All the experiments are conducted from April 1 to April 30, 2009, using the same initial and boundary conditions with the same model domain and parameterizations. April 2009 was chosen because a very strong MJO event propagated across the MC (Figure 1c, LaFleur et al., 2015; Moncrieff, Waliser, & Caugley, 2012; Moncrieff, Waliser, Miller, et al., 2012; Waliser et al., 2012). The spring season is also the time when the MJO is typically closest to the equator (Zhang & Dong, 2004). Based on Densmore et al. (2019), this MJO event was an active-active (AA) event, that is, an event that entered the MC in phase 4 with a Real-time Multivariate MJO (Wheeler & Hendon, 2004) amplitude greater than 1.0 and maintained amplitude of 1.0 or greater through its exit of the MC in phase 5. Using long-term data, Densmore et al. (2019) also found that 50% of the MJO events that propagate through MC are AA. Therefore, our chosen MJO event can arguably be considered typical. The extent to which our results are valid for other similar events or events that are weak (i.e., do not propagate over the MC) should be tested in the future.

For model evaluation, winds at 850 hPa are taken from the ERA-Interim reanalysis, and rainfall is taken from the Climate Prediction Center morphing technique (CMORPH, 8 km × 8 km, 30 min; Joyce & Xie, 2011) data set. Precipitable water data are from the MODIS Level 3 atmospheric products (MOD 08, 1° × 1°, Platnick et al., 2015).

3. Results

3.1. Large-Scale Structure

The observed precipitation during April 2009 shows a wide maximum over the tropical warm pool area, with the InterTropical Convergence Zone (ITCZ) between the equator and 10°N (Figure 2a). There are notable maxima in precipitation over islands of Borneo and New Guinea, and near the southern part of Sumatra. The CTL simulation captures this distribution (Figure 2c), although it underestimates precipitation over the ocean (4.52 mm day^{-1} in CTL and 5.66 mm day^{-1} in observation) and overestimates over the

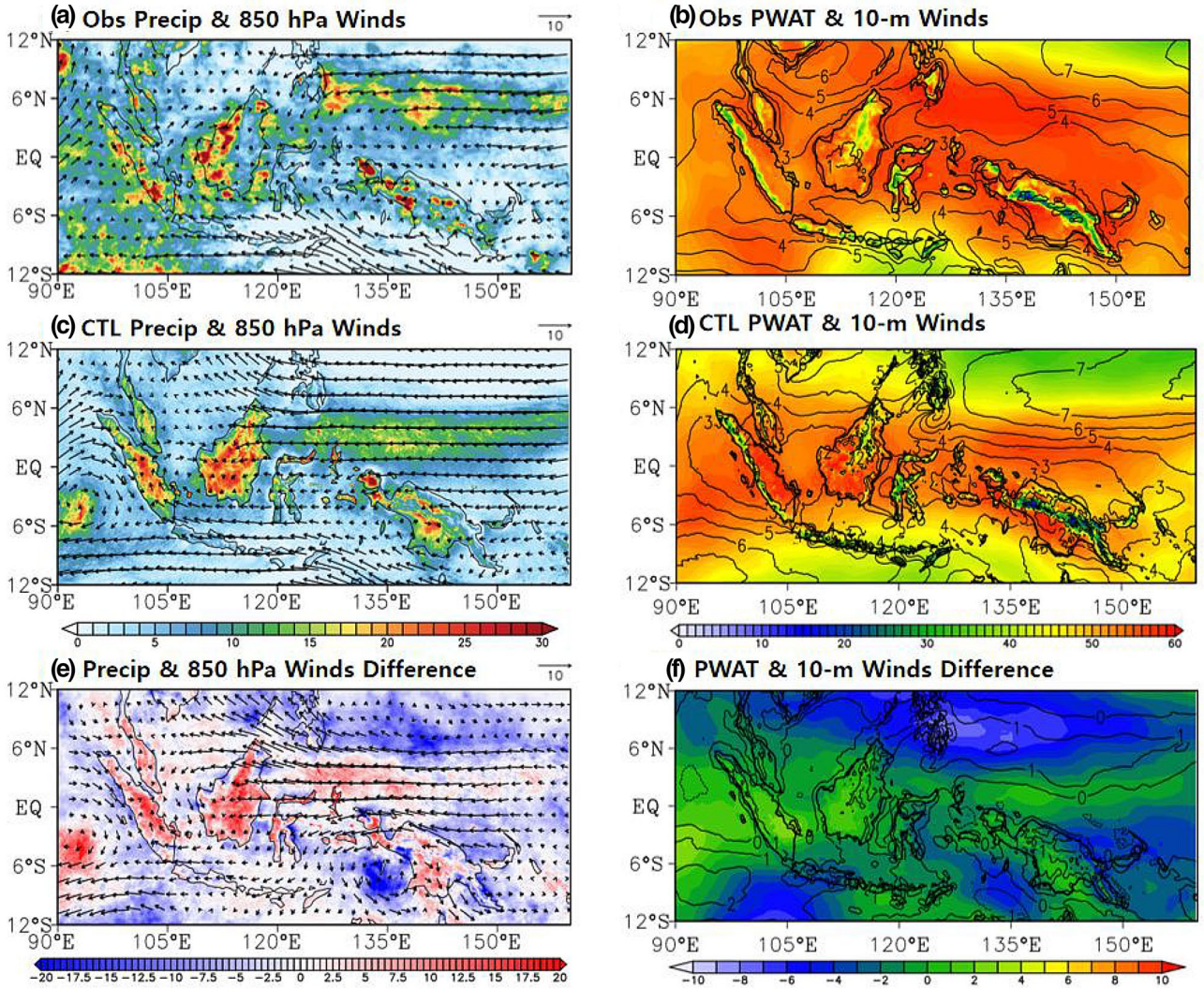

Figure 2. (Left) Mean precipitation (mm day^{-1}, shaded) and horizontal winds (m s^{-1}, vector) at 850 hPa from the (a) observations (CMORPH and ERA-Interim), (c) CTL simulation, and (e) their difference (CTL minus observations) for April 2009. The right panels are mean precipitable water (PWAT, mm, shaded) and winds at 10-m (m s^{-1}, contour) from the (b) observations (MODIS Level 3 atmospheric products and ERA-Interim), (d) CTL simulation, and (f) CTL minus observation.

islands (9.92 mm day^{-1} in CTL and 7.66 mm day^{-1} in observation). The overestimation over the islands in CTL shows spatially widespread precipitation instead of being confined to specific regions as seen in observations. This is likely due to the convective scheme that readily triggers over land thus producing higher precipitation. The observed precipitation over Borneo shows a dipolar pattern (drier in the east half and wetter in the west half; Qian, 2019; Wei et al., 2020) that is partly captured in the CTL simulation. On the other hand, a dry bias is noticed over the ocean, with a much smoother ITCZ structure over the western Pacific Ocean and a noticeably dry bias over the eastern Indian Ocean. Similar precipitation bias has been found in previous studies (e.g., Argüeso et al., 2019; Birch et al., 2016; Gianotti et al., 2012; Im & Elthair, 2018; Kwan et al., 2013; Leutwyler et al., 2017). In particular, the dry bias over the ocean is evidently a characteristic problem of models (Love et al., 2011). Argüeso et al. (2019) found that the improvement using higher model resolution was limited when simulated over a large domain in the MC, but considerable improvement was achieved over areas with higher topography (>=1,000 m) at 2-km resolution. One should also note that the satellite observations have their own bias as well (Ebert et al., 2007; Huffman et al., 2007; Skok et al., 2016; Vincent & Lane, 2016; Yilmaz et al., 2005). For example, Hassim et al. (2016) compared the model simulation with ground-based radar and found that the model matched well with the radar, suggesting that at

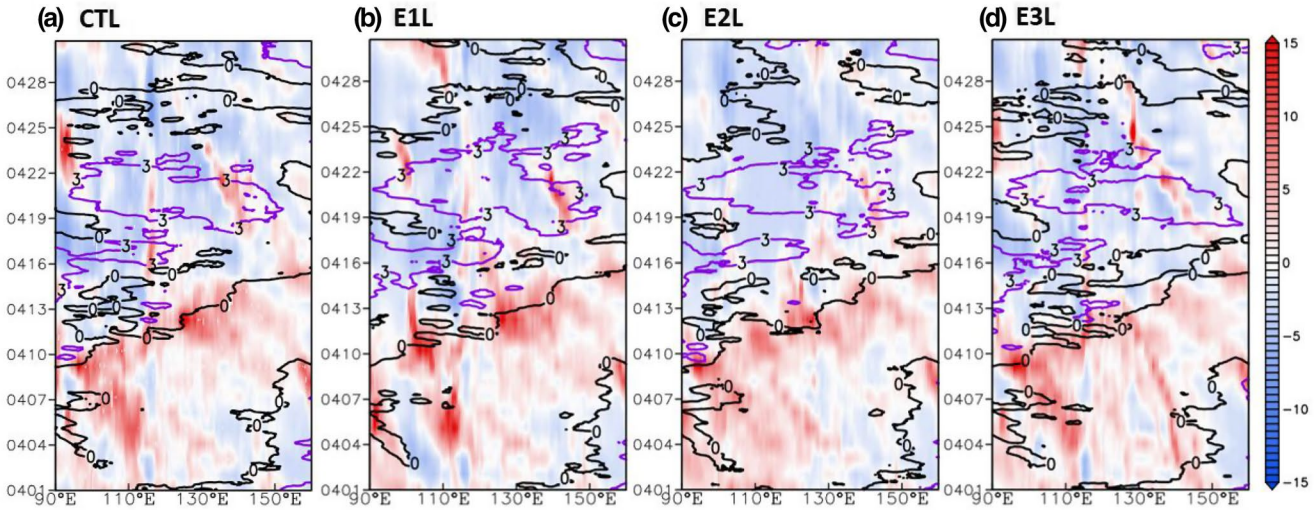

Figure 3. Time-longitude diagrams (averaged over 10°S–10°N) of daily anomalies of zonal winds at 850 hPa (contours, only 0 and 3 m s^{-1} are shown) and precipitation anomaly (shaded, mm day^{-1}) from the (a) CTL, (b) E1L, (c) E2L, and (d) E3L.

least some discrepancy may come from the lag in the satellite data (e.g., Kikuchi & Wang, 2008; Rauniyar & Walsh, 2013).

The most distinct difference in horizontal winds at 850 hPa between the CTL and reanalysis occurs to the west of Sumatra, north of Borneo, and New Guinea, where the CTL shows stronger winds (Figure 2e). The precipitable water (PWAT) in the CTL experiment (Figure 2d) is similar to the observations from MODIS (Figure 2b), but a dry bias exists over the off-equatorial western Pacific Ocean north of 5°N (Figure 2f). There is a wet bias over the eastern Indian Ocean and central MC possibly due to moisture advection that modifies the localized PWAT. The mean 10-m wind in the reanalysis is fairly well captured in the CTL simulation also (Figure 2, right panels). In general, however, the bias in easterlies is larger over the western Pacific Ocean, possibly due to the use of coarse horizontal resolution (e.g., Tan et al., 2020), the model domain not big enough to accommodate Rossby gyres (e.g., Ray et al., 2012), or to the lack of air–sea interactions (e.g., Flatau et al., 1997; Sobel et al., 2010; Zhou et al., 2020), among others. The bias in precipitation over smaller islands like Java (1.94 mm day^{-1}) and Sulawesi (2.21 mm day^{-1}) is perhaps because these islands are underresolved in the model. During the MJO propagation through MC, the observed transition from easterly to westerly winds at 850 hPa is well simulated in all experiments (Figure 3), providing confidence in studying the variation in precipitation in these sensitivity experiments. The bias in winds at 850 hPa and at the surface is prominent in the eastern Indian Ocean. Whether this discrepancy is caused by the model physics or lower spatial resolution will require further investigation.

The easterly and westerly phases (anomaly winds) in models (Figure 3) are well simulated when compared with observations (Figure 1c). The transition of zonal winds at 850 hPa from easterly anomalies to westerly anomalies, and of precipitation anomalies from negative to positive, indicates the arrival of MJO in the MC and is consistent with the outgoing longwave radiation-based MJO index (OMI, Kiladis et al., 2014). The positive anomalies in U850 and precipitation propagated eastward during the MJO event, with interruptions by the landmass indicating the influence of the islands. The eastward-propagating westerlies at 850 hPa are evident in both reanalysis (Figure 1c) and simulations (Figure 3). The eastward propagation of the simulated precipitation, however, is faster than observations. This common concern in WRF simulations of the MJO indicates a deficiency of the coupling between the circulation and convection in the model compared to observations (e.g., Hagos & Leung, 2011; Holloway et al., 2013; Hung et al., 2013; Lin et al., 2006; Ray et al., 2009; Wang et al., 2015). The easterly and westerly phases in observations during April are recognized as 1–13 for easterly and 14–30 for westerly over Sumatra; 1–15 for easterly and 16–30 for westerly over Borneo; and 1–17 for easterly and 18–30 for westerly over New Guinea. The easterly and westerly phases considered in April 2009 in model simulations areas are 1–10 for easterly and 11–26 for

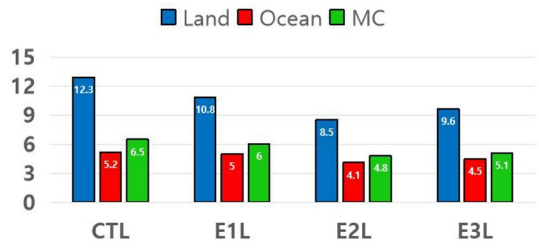

Figure 4. Precipitation over land (blue), ocean (red), and entire MC (green) from the CTL (control), E1L (removal of Sumatra), E2L (removal of Borneo), and E3L (removal of New Guinea) for April 2009. Unit in mm day^{-1}. MC, Maritime Continent.

westerly over Sumatra; 1–11 for easterly and 12–26 for westerly over Borneo; and 1–13 for easterly and 14–26 for westerly over New Guinea. The above dates from model simulations differ slightly from the reanalysis winds (Figure 1c) due to small differences between the observations and simulations. Adjusting these dates does not change the results or conclusions in the study.

The precipitation over islands, water, and the entire MC for each experiment (Figure 4) illustrates that removal of Borneo has the largest impact on precipitation: a decrease from 12.3 to 8.5 mm day^{-1} over land and 5.2 to 4.1 mm day^{-1} over ocean. Although New Guinea is the largest island in the MC, its removal does not invoke the strongest precipitation response. This suggests that the island size alone does not play a key role in the total precipitation.

During the background lower-tropospheric easterlies, the CTL simulation shows strong precipitation over Sumatra and Borneo Islands (Figure 5a). Removal of individual islands causes changes in precipitation over the neighboring islands (Figures 5c, 5e, and 5g). For example, when Borneo is removed (E2L), precipitation over Sumatra is reduced (Figure 5e). Similarly, when New Guinea is removed (E3L), precipitation over Sumatra and Borneo is reduced (Figure 5g). Both these experiments indicate that precipitation decreases to the west of the removed island in the presence of easterlies. Moreover, the easterlies between Sumatra and Borneo become stronger in the E2L (removal of Borneo) than in the CTL simulation. Thus, a systematic reduction in precipitation over an island to the west of the removed island occurs in the presence of background easterlies, but there is no systematic pattern in precipitation to the east of the removed island (Table 1).

During the westerly lower-tropospheric winds associated with MJO (Figures 5d, 5f, and 5h), the pattern in precipitation change is distinct and systematic: when an island in the MC is removed, the islands to its east receive more precipitation, and the islands to its west receive less precipitation. When the islands are removed, the westerlies become stronger to the east of the removed islands. For example, in the absence of Sumatra (E1L), the stronger westerlies between Sumatra and Borneo (Figure 5d) cause more precipitation over Borneo compared to CTL. The Froude number is smaller ($F_r < 0.2$) for both westerly and easterly phases over Sumatra, which is consistent with earlier results (e.g., Qian, 2019; Riley Dellaripa et al., 2019). This low F_r indicates that the flow from the west or the east is unable to pass over the Sumatra mountains (Figure 5d). During the westerly phase when Sumatra is removed (E1L), the lack of land convection over Sumatra and the lack of blocking by land and topography lead to an increase in westerlies to the east of Sumatra (Figure 5d). However, the flow pattern to the west of Sumatra is more complex. Evidently, the wind response due to lack of land convection over Sumatra cancels the blocking effect. The extent to which this flow pattern is modulated by the diurnal cycle needs to be investigated in the future.

Similarly, when Borneo is removed (E2L), the stronger westerlies between Borneo and New Guinea (Figure 5f) increase the precipitation over New Guinea. On the other hand, easterlies between Sumatra and Borneo lead to a reduction of precipitation over Sumatra (Figure 5f). In the absence of New Guinea (E3L), anomalous easterlies between Sumatra and New Guinea decrease precipitation over both Sumatra and Borneo (Figure 5h).

The patterns in precipitation in these sensitivity experiments relative to the control are summarized in Table 1. Clearly, there is a systematic pattern in change in precipitation during the westerlies: removal of an island increases precipitation over an island located to its east, whereas precipitation decreases over an island located to its west. This behavior is consistent with the response in circulation to heating in the tropics (e.g., Gill, 1980; Matsuno, 1966) that generates Rossby waves to the west of the heating accompanied by lower-tropospheric westerlies, and Kelvin waves to the east accompanied by easterlies (e.g., Rui & Wang, 1990). In the absence of latent heating, for example over Borneo when Borneo is removed (E2L), the westerlies become weaker to the west, and the easterlies become weaker to the east (Figure 5f). As a result, precipitation over Sumatra decreases, and precipitation over New Guinea increases in the absence of

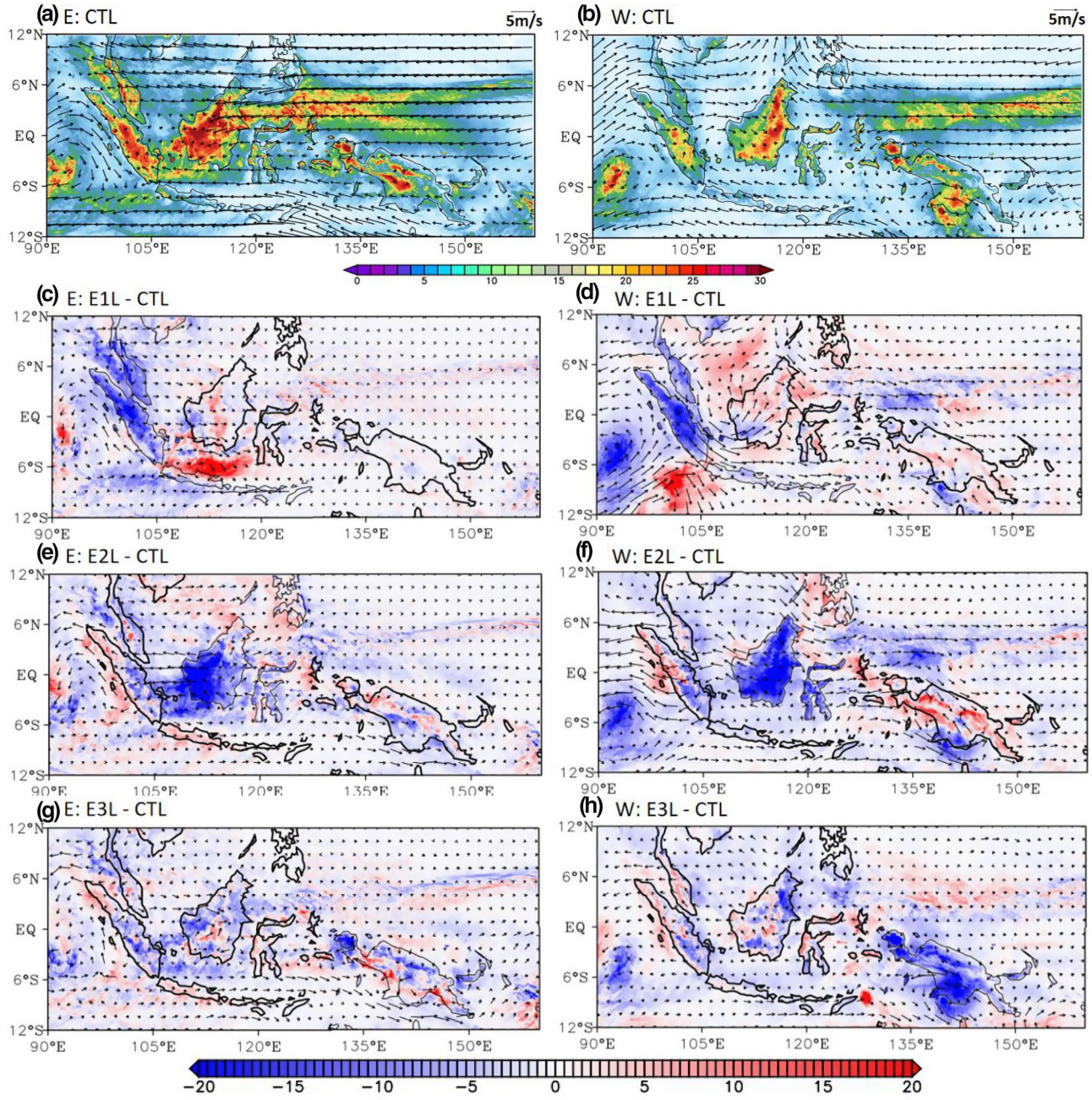

Figure 5. Precipitation (mm day^{-1}, shaded) and horizontal winds at 850 hPa (m s^{-1}, vector) from the (a) CTL, (c) E1L (removal of Sumatra) minus CTL, (e) E2L (removal of Borneo) minus CTL, and (g) E3L (removal of New Guinea) minus CTL during the easterly (E) anomaly period. Right panels (b, d, f, and h) are during the westerly (W) anomaly period. The removed islands are plotted with lighter black lines.

Borneo because tropical convection is preferred in the presence of background westerlies (see Section 4). To understand the underlying processes that lead to this precipitation pattern over islands during background westerlies during MJO propagation and during background easterlies prior to MJO arrival, we conduct a moisture budget analysis as follows.

Table 1
Precipitation Change (%) in sensitivity experiments compared with CTL simulation over individual islands during easterly (E) and westerly (W) lower-tropospheric winds.

Versus CTL Precip during E	Sumatra Islands	Borneo & Sulawesi Islands	New Guinea Islands
E1L (%)		3%↑	7%↓
E2L (%)	12%↓		**24%↓**
E3L (%)	10%↓	6%↓	
Versus CTL Precip during W	**Sumatra Islands**	**Borneo & Sulawesi Islands**	**New Guinea Islands**
E1L (%)		6%↑	**14%↑**
E2L (%)	**12%↓**		**27%↑**
E3L (%)	13%↓	**21%↓**	

Note. The upward arrows show increase and downward arrows show decrease in precipitation. The percentage represents the change in precipitation compared to the CTL simulation, and the bold percentage shows when the change in precipitation is statistically significant at 95% confidence limit using a Student's *t* test. The magnitude of change in precipitation can be found in Figure 5.

3.2. Physical Processes

We use a column-integrated moisture budget analysis (e.g., Hsu & Li, 2012; Ray & Li, 2013; Wang et al., 2015) given by

$$\left\langle \frac{\partial q}{\partial t} \right\rangle = -\left\langle v_h \cdot \nabla q \right\rangle - \left\langle \omega \frac{\partial q}{\partial p} \right\rangle + E - P + R \tag{1}$$

where q is the specific humidity, v_h is the horizontal wind, ω is the vertical velocity, E is the evaporation, P is the precipitation, and R is the residual. The $< >$ notation indicates a mass-weighted vertical integral from surface to 100 hPa. The term on the left-hand side is the moisture tendency, and the first and second terms on the right-hand side are the horizontal (HADV) and vertical advection (VADV), respectively.

When an island is replaced with water, the precipitation over the removed island decreases substantially compared to the CTL simulation due to a decrease in VADV and HADV (Figure 6). For example, during the easterly phase, the precipitation decreased from 17 mm day^{-1} in CTL to 2.4 mm day^{-1} in E2L over Borneo due to a decrease in VADV (11.9 to 1.97 mm day^{-1}) and HADV (3.6 to −0.4 mm day^{-1}). Interestingly, evaporation also decreased from 1.51 to 0.80 mm day^{-1}) in E2L during the easterly phase due to a decrease in winds over the removed island.

During the easterly phase (Figure 7), horizontal wind-induced vertical uplift (i.e., vertical advection) is smaller due to divergence of the winds due to Coriolis. The increase in easterlies may, however, increase the horizontal advection of moisture and evaporation, but their magnitudes are found to be smaller compared to the vertical advection of moisture. As an overall result, a small change in vertical advection can compensate a larger change in other terms in the moisture budget. Taking E2L (removal of Borneo) as an example: during the easterly phase, the difference in precipitation between the CTL and E2L over Sumatra Islands is −2 mm day^{-1} (E2L minus CTL), which is balanced by evaporation (−0.75 mm day^{-1}), VADV (−2 mm day^{-1}), and HADV (0.91 mm day^{-1}). The increase in HADV is due to increased winds, and the decrease in evaporation is due to a decline in the sea-air humidity difference even in the presence of increased easterlies. Similarly, while an increase in easterlies (see Figure 5e between Sumatra and Borneo) leads to an increase in HADV, it does not increase VADV because of the divergence by Coriolis. These results are similar in E3L (removal of New Guinea) during easterlies, except for the HADV term, which decreases over both Sumatra and Borneo. This decline in HADV is due to a decrease in the horizontal gradient in humidity (∂q / ∂x).

During the background westerlies (Figure 8), precipitation over an island increases when adjacent islands to its west are removed; precipitation over an island decreases as adjacent islands to its east are removed. An increase in precipitation compared with CTL over the islands during MJO-associated westerly winds is due

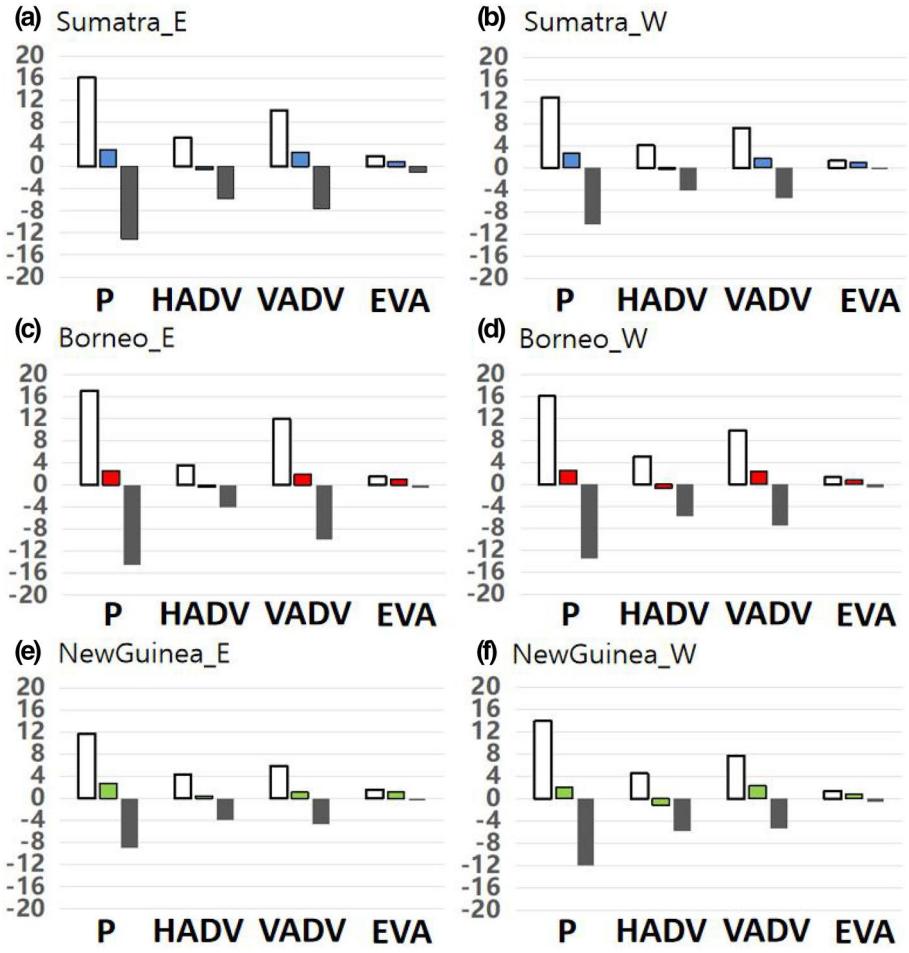

Figure 6. (Top) Moisture budget for the CTL (white), E1L (blue), and E1L minus CTL (black) over Sumatra during (a) easterly (E) and (b) westerly (W) phases. The middle panels (c and d) are for CTL and E2L (red bar) over Borneo and the bottom panels (e and f) are for CTL and E3L (green bar) over New Guinea. Unit in mm day^{-1}.

to the increase of VADV. When islands have less precipitation during the westerly phase, the contributions are from VADV and evaporation. For example, during the westerly phase in E1L, precipitation over Borneo and New Guinea Islands increases by 6% (1 mm day^{-1}) and 14% (1.59 mm day^{-1}). However, the change in precipitation over Borneo was not statistically significant at the 95% confidence level based on the Student's *t* test. In the absence of Borneo (E2L), 12% (1.55 mm day^{-1}) decrease in precipitation over the Sumatra Islands (Figures 8d) and 27% (3.15 mm day^{-1}) increase in precipitation over the New Guinea Islands (Figure 8f) were mostly due to VADV, and these changes in precipitation were found to be statistically significant. The absence of New Guinea Islands (E3L) causes precipitation decrease over Borneo by 21% (3.33 mm day^{-1}) (Figure 8h) and over Sumatra by 13% (1.64 mm day^{-1}) (Figure 8g) due to a decrease in VADV and evaporation. This indicates that in the absence of islands, the precipitation variation during MJO-associated westerlies is strongly linked to VADV and is clearer in E2L than E1L. This is possibly because Sumatra being smaller than Borneo may not excite a large-scale response as strong as Borneo. Also, note that the precipitation over land in the MC decreases by 16%, 33%, and 25% in E1L, E2L, and E3L experiments, respectively.

The extent to which the change in precipitation over the surrounding islands due to lack of land convection over a removed island is a direct result from change in large-scale circulations, or an indirect result from change in local circulations (e.g., land-sea breeze), or due to upscale transport by organized convection that affect the MJO itself (e.g., Moncrieff, 2019) would be topics of interest in the future. One of the main issues in our coarse resolution simulation is that they may not be able to faithfully capture the land-sea breeze that controls the diurnal cycle of precipitation, leading to bias in the simulated diurnal cycle of precipitation

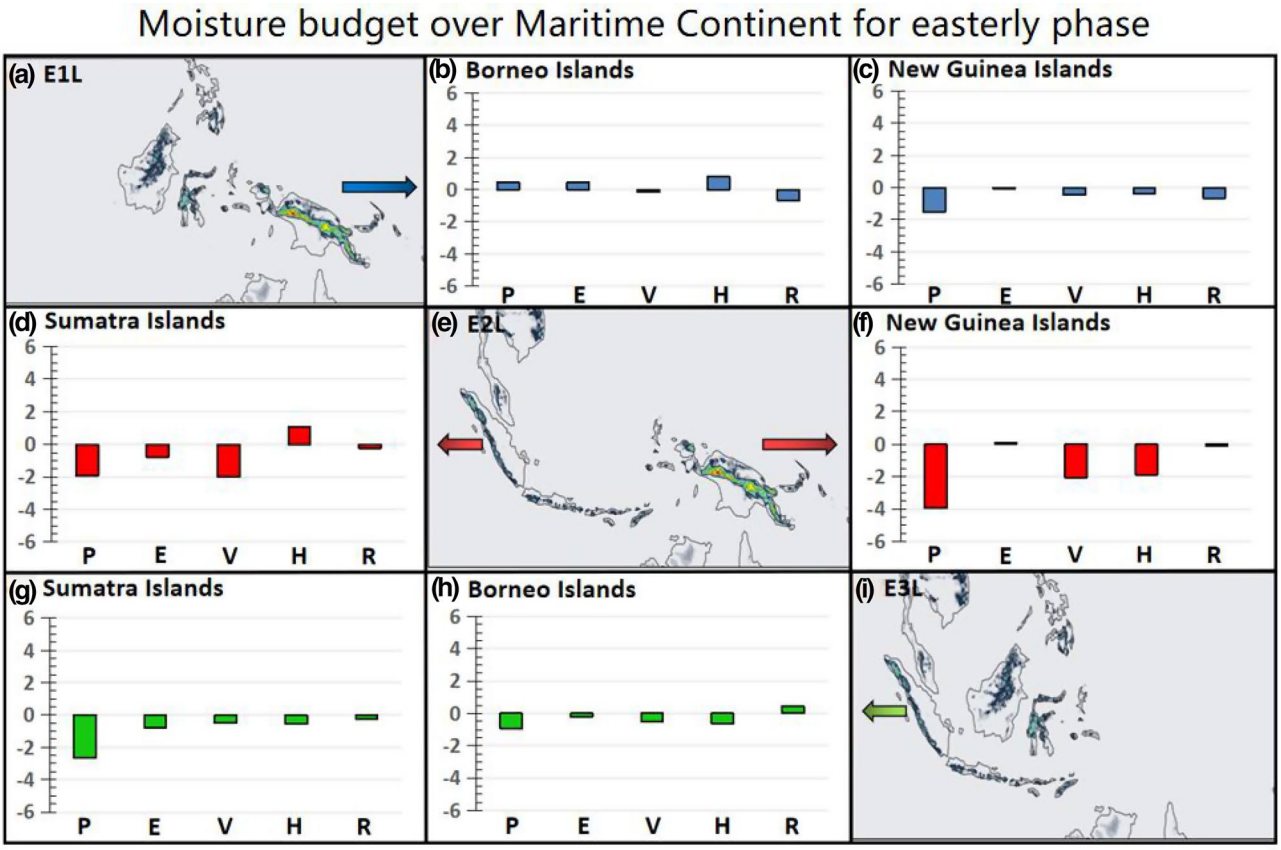

Figure 7. (a) Graphical representation of the numerical experiment E1L (removal of Sumatra, blue bar). (b) The column-integrated (1,000–100 hPa) moisture budget terms for E1L minus CTL over Borneo and (c) New Guinea. The middle panels are for the experiment E2L (removal of Borneo, red bar), and the bottom panels are for E3L (removal of New Guinea, green bar). All are during period of background easterlies, the exact timing of which can be found in text. The terms P, E, V, H, and R represent precipitation, evaporation, vertical moisture advection (VADV), horizontal moisture advection (HADV), and residual, respectively. The shadings in (a, e, and i) show topography (see Figure 1a for topographic height). Unit for bar charts: mm day^{-1}.

in the model (not shown). This is certain to impact the diurnal gravity waves which are excited and maintained directly by latent heating from mesoscale convective systems over land (Ruppert et al., 2020). Ruppert and Zhang (2019) speculated that the synchronized diurnal forcing of Sumatra and Borneo due to their proximity benefits stronger gravity wave response compared to if the islands were isolated. The absence of topography has only a secondary impact on the mesoscale convective systems and gravity waves (Ruppert & Chen, 2020)

4. Discussion and Conclusion

The role of land-sea contrast on an MJO event during April 2009 in the MC is explored during both easterly and westerly background winds using four numerical experiments: a control simulation (CTL) and simulations without the islands of Sumatra (E1L), Borneo (E2L), and New Guinea (E3L). To explain the role of land-sea contrast on precipitation during the easterly and westerly winds, a moisture budget analysis is conducted over three major islands in the MC: Sumatra, Borneo and Sulawesi, and New Guinea. The main results of this study are as follows:

1. In the presence of background lower-tropospheric easterlies, precipitation decreases in the islands to the west of the removed island due to increased moisture divergence generated by the easterlies. In the absence of surface friction and reduced latent heating of condensation due to reduced precipitation, easterlies become stronger, leading to a decrease in vertical/horizontal moisture advection (E2L and

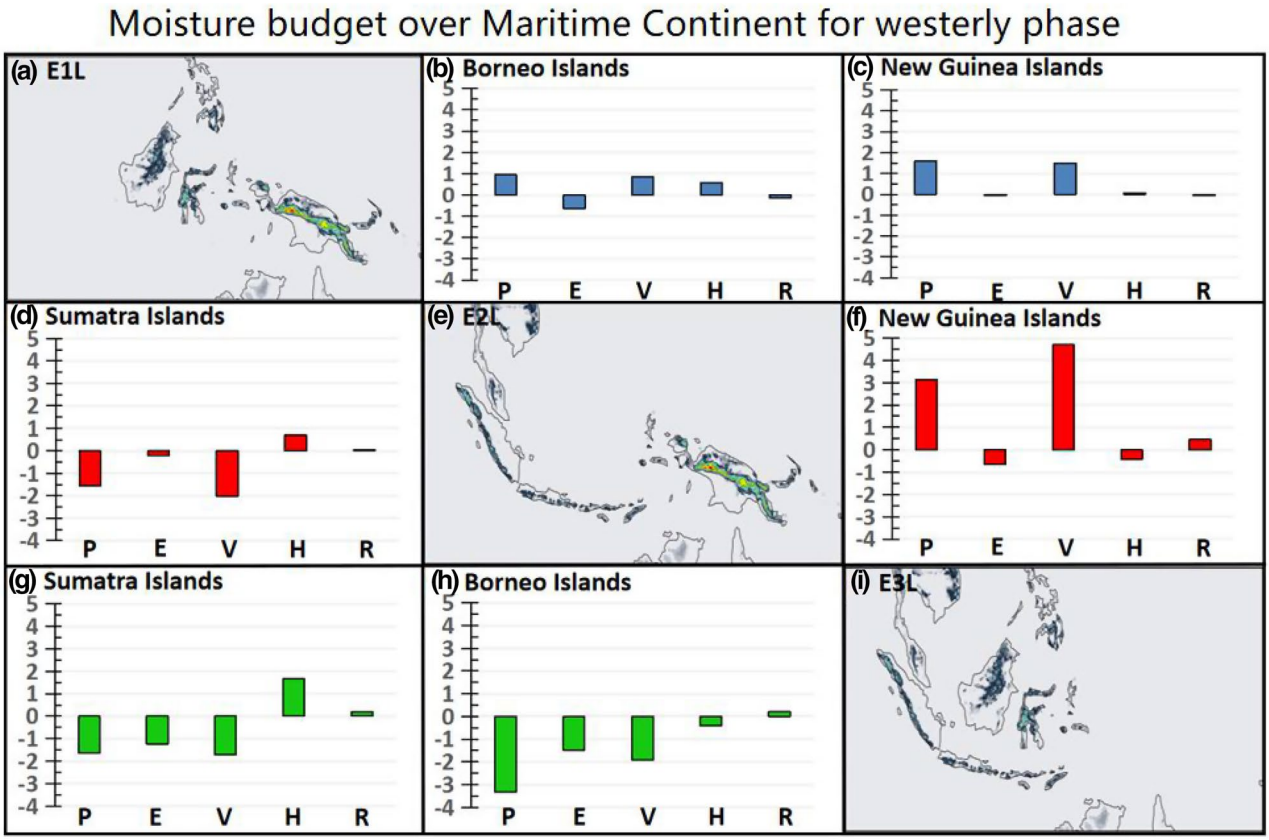

Figure 8. Same as Figure 7 but during the background westerlies.

E3L) and precipitation over the islands to the west of the removed island. On the other hand, the divergence of the winds due to Coriolis induces less vertical advection. The reduction in precipitation over the removed land stems from decreased surface heating from incoming solar radiation and the larger heat capacity of water.

2. During the westerly lower tropospheric winds associated with the MJO, the change in precipitation over land is distinct and systematic: when an MC island is removed, the islands to its east receive more precipitation and the islands to its west have less precipitation (Table 1 and Figure 9) for two reasons. First, in the absence of friction and obstruction over land and its topography, the westerlies become stronger to the east of the removed island (Figure 9b). Second, the decrease in latent heating over the removed island due to decrease in precipitation decreases the westerly anomaly to the west, and easterly anomaly to the east, follows the classic theory of Gill (1980). The above processes lead to an increase in westerlies to the east resulting in increased vertical advection of moisture and an increase in precipitation (Figure 8) by about 16% on average over the islands to the east of the removed island (Figure 9b). On the other hand, decrease in westerlies to the west of the removed island leads to a decrease in precipitation (about 10% over MC, Figure 9b). Note that the near-equatorial convection is preferred over the background westerlies because Coriolis force increases the westerly convergence (Figure 9c).

Moreover, the westerlies also lead to oceanic downwelling due to Ekman transport causing warmer SST near the equator. On the other hand, these westerlies can induce more ocean evaporation and upper ocean mixing, both of which contribute to SST cooling. Additionally, the complex bathymetry in the MC also controls the SST variability. For example, the water is shallow and warm between Java, Sumatra, and Borneo, where upwelling or mixing is not effective; whereas, the water is much deeper between Sulawesi and New Guinea where upwelling/downwelling, and wind-driven mixing play a pivotal role in SST variability (Iskandar, 2010; Kida & Richards, 2009; Rachman et al., 2020). Tests of these mechanisms require a

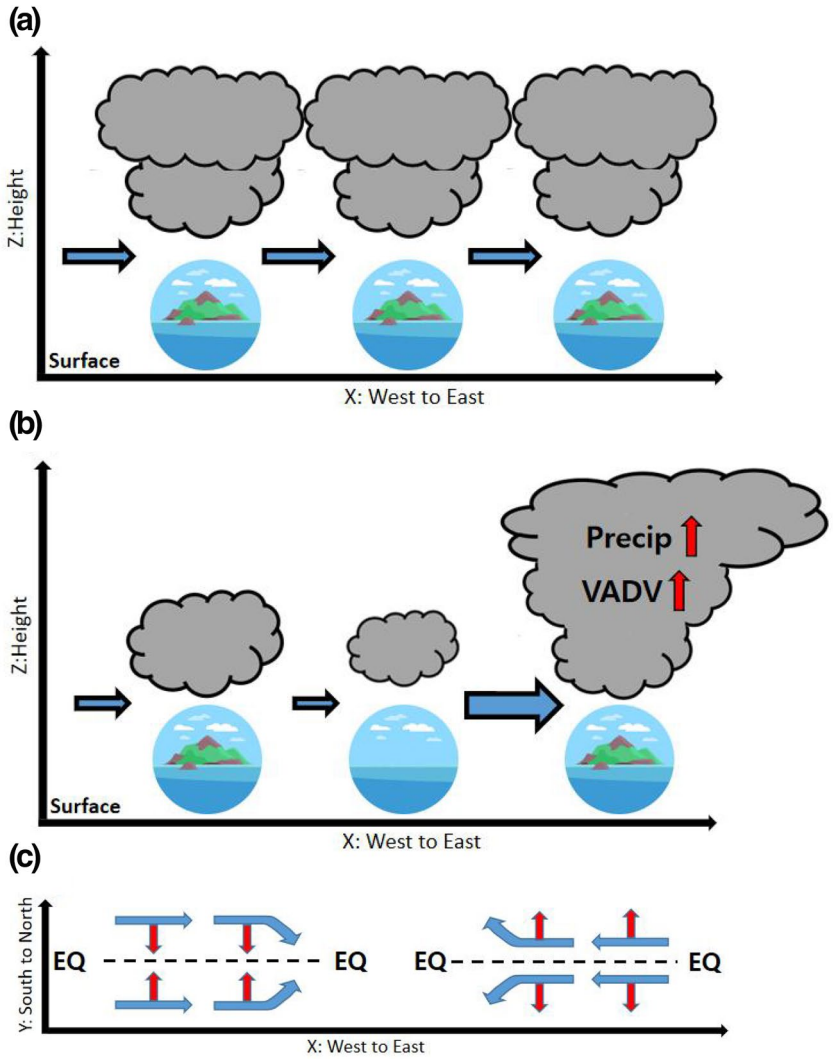

Figure 9. (a) Schematic of precipitation over three islands located along the equator during the MJO propagation with background lower-tropospheric westerly winds (shown by the blue arrows). (b) Precipitation over the three islands when the middle island is removed. In the absence of friction and obstruction by land, and reduced latent heating over the removed island, westerlies become stronger to the east of the removed island leading to an increase in vertical advection of moisture (VADV) and precipitation over the island to the east of the removed island. On the other hand, the precipitation decreases in the island to the west of the removed island. The cloud size represents the convection/precipitation. (c) Schematic of the mechanism of near-surface convergence in the presence of westerlies and near-surface divergence in the presence of easterlies near the equator. The cloud size represents the convection/precipitation. The red arrows in (c) denote the Ekman transport. EQ stands for equator. MJO, Madden–Julian Oscillation.

coupled ocean-atmosphere model and that is beyond the scope of this study. When an island is removed during surface westerlies, changes in nearby precipitation mostly stem from changes in HADV and VADV (Figure 8). Increases in precipitation are mostly dominated by VADV but decreases in precipitation are controlled by both horizontal (HADV) and vertical moisture advection (VADV) (Figures 8 and 9).

There are a few aspects of this study that need further discussions.

i. The implied role of land-sea contrast in this study arguably comes from both the land surface properties and topography. In particular, a recent study by Jiang et al. (2019) using the ERA-5 reanalysis (Hersbach et al., 2020) has shown that precipitation associated with the MJO is collocated with the topographic features in the MC. On the other hand, Ruppert and Chen (2020) using numerical simulation found that

the basic-state forcing by land is the only factor that substantially enhances total rainfall amount over the islands in the MC. Wang and Sobel (2017) found a nonmonotonic relationship between prevailing winds and precipitation in their highly idealized islands. The thermally forced circulation associated with the sea breeze is strong when the prevailing winds are weak, but it weakens with increasing wind speed as horizontal advection of temperature reduces the land-sea temperature contrast, while mechanically forced gravity waves associated with surface inhomogeneity strengthen with wind speed. As a result, the change in the circulation regimes with wind speed leads to the nonmonotonic behavior in precipitation. During the easterly phase, in the presence of weaker prevailing winds, the diurnal cycle in precipitation is stronger than that during the westerly phase in the presence of stronger prevailing winds and is particularly evident over Sumatra in our simulations (not shown). This result is consistent with Wang and Sobel (2017). However, a decrease in precipitation diurnal cycle is not apparent from easterly to westerly phase over Borneo and New Guinea in both observations and model simulations (not shown), indicating that added complexity may alter the idealized results of Wang and Sobel (2017). More work in the future is needed to fully understand the model behavior concerning its diurnal cycle in precipitation.

ii. We have invoked the Gill model to describe and interpret part of our results. The spatial extent of heating over the islands is small, in particular over Sumatra, and the Gill solution may not be well suited. Apart from the scales of heating, Gill model also had a number of other simplifications (e.g., linear with a simple damping term, no land, etc.). As a result, a clear Gill response in our full physics model with topography and other complexities is not expected. But, even with so many differences, the similarity of our results to the Gill model is surprising. For example, Sumatra being a smaller island may not be able to excite a Kelvin–Rossby response that is as strong as that by Borneo. On the other hand, the E2L experiment (removal of Borneo, Sulawesi, and the surrounding islands) leads to a much stronger wind response than in E1L (Table 1) presumably because the overall size of the removed islands in E2L is much larger than that in E1L.

iii. During the westerlies, an increase in convection over an island located to the east of the removed island is due to the combined effect of Gill response and removal of the physical obstacle that allows westerlies to propagate further east. The separation and quantification of the influence of these two processes on precipitation, and how they may be further influenced by the diurnal cycle warrants further study in the future because, we are yet to have a consensus regarding the MJO–diurnal cycle association. Some studies have suggested that the MJO diminishes the diurnal cycle during active phase and enhances the diurnal cycle during the suppressed phase (Rauniyar & Walsh, 2011; Sui & Lau, 1992; Sui et al., 1997). On the other hand, studies have shown that the diurnal cycle of deep convection over land is enhanced during the active MJO compared to the suppressed MJO phase (Lu & Wang, 2019; Oh et al., 2012; Suzuki, 2009; Tian et al., 2006).

iv. Although we simulated a single MJO event over a short time period, our results may help understand the distribution of climatological precipitation patterns in the MC. For example, when Borneo (E2L) and New Guinea (E3L) are removed, the precipitation is reduced substantially over the islands of Sumatra (Figures 7 and 8 and Table 1). This indicates that Sumatra receives more precipitation due to the presence of Borneo and New Guinea, irrespective of whether background winds are easterlies or westerlies. Similarly, Borneo receives less precipitation due to the presence of Sumatra but more precipitation due to the presence of New Guinea. Overall, however, the influence of New Guinea on Borneo seems to be more dominant than Sumatra, leading to an increase in precipitation over Borneo due to the presence of neighboring islands. On the other hand, New Guinea receives more precipitation during easterlies and less precipitation during westerlies in Sumatra and Borneo's presence. Therefore, the net effect of other islands on precipitation climatology over New Guinea depends upon the relative timespan and intensity of rainfall during the easterlies and westerlies. This statement can be tested using similar simulations but over a much longer period. We plan to follow this line of research in the near future.

In short, despite competition for moisture among neighboring islands (e.g., Qian, 2007), the presence of a large number of islands in the MC provides a more conducive environment for increased precipitation in the MC islands. Our results are consistent with Sarr et al. (2019), who in a paleoclimate study showed that the Sunda shelf induced an increase in seasonal rainfall cycle over itself, with higher precipitation rates

during the transitional rainy season. The shelf's response is characterized by the seasonal enhancement of moisture convergence and continental precipitation driven by the land surface's thermal properties. Sarr et al. (2019), however, did not estimate the effect of the Sunda shelf on neighboring islands.

In summary, it is known that precipitation over an island in the MC depends on the surrounding islands due to competition between them for moisture from the ocean (e.g., Qian, 2007). In this study, we show that this precipitation variation depends on the background winds (easterly or westerly) because the background winds change the physical processes that control precipitation over the islands (Figure 5). In addition, westerly winds supply increased moisture. Since the precipitation and its diurnal cycle can have an influence on the propagation of the MJO (Kanamori et al., 2012; Oh et al., 2012; Peatman et al., 2014; Rauniyar & Walsh, 2011), understanding of the role of land-sea contrast can improve the representation of physical processes in the model. Further studies regarding the interaction between the land-sea contrast and diurnal cycle of precipitation are required for better understanding and a more accurate forecast of the MJO. One particular implication of our results is that the model bias in precipitation over an island may come from the model bias in precipitation from surrounding islands and their representations in the model. Therefore, higher-resolution models that can represent better land-sea contrast and better use of high-resolution topography data sets may improve the model simulation over the MC.

Data Availability Statement

Data sets used in this study include ERA-Interim reanalysis data (https://www.ecmwf.int/en/forecasts/datasets/reanalysis-datasets/era-interim) and Climate Prediction Center Morphing Technique (https://ftp.cpc.ncep.noaa.gov/precip/CMORPH_V1.0/CRT/8km-30min/). Precipitable water data are from the MODIS Level 3 atmospheric products (https://atmosphere-imager.gsfc.nasa.gov/products/water-vapor).

Acknowledgments
This study was supported by the ONR awards N00014-1601-3091 to P.R. and N0001416WX01752 to B.B. We would also like to acknowledge high-performance computing support from Cheyenne (doi:10.5065/D6RX99HX) provided by NCAR's Computational and Information Systems Laboratory, sponsored by the National Science Foundation. Constructive comments from five anonymous reviewers improved the manuscript.

References

Ahn, M. S., Kim, D., Kang, D., Lee, J., Sperber, K. R., Gleckler, P. J., et al. (2020). MJO propagation across the Maritime Continent: Are CMIP6 models better than CMIP5 models? *Geophysical Research Letters*, *47*, e2020GL087250. https://doi.org/10.1029/2020GL087250

Ajayamohan, R. S., Khouider, B., & Majda, A. J. (2013). Realistic initiation and dynamics of the Madden–Julian Oscillation in a coarse resolution aquaplanet general circulation model. *Geophysical Research Letters*, *40*, 6252–6257. https://doi.org/10.1029/2013GL058187

Argüeso, D., Romero, R., & Homar, V. (2019). Precipitation features of the Maritime Continent in parameterized and explicit convection models. *Journal of Climate*, *33*, 2449–2466. https://doi.org/10.1175/JCLI-D-19-0416.1

Birch, C., Webster, S., Peatman, S., Parker, D., Matthews, A., Li, Y., & Hassim, M. (2016). Scale interactions between the MJO and the western Maritime Continent. *Journal of Climate*, *29*, 2471–2492. https://doi.org/10.1175/JCLI-D-15-0557.1

Chen, F., & Dudhia, J. (2001). Coupling an advanced land surface hydrology model with the Penn State–NCAR MM5 Modeling System. Part I: Model implementation and sensitivity. *Monthly Weather Review*, *129*, 569–585.

Chou, M. D., & Suarez, M. J. (1994). An efficient thermal infrared radiation parameterization for use in general circulation models. *NASA Tech. Memo*, *104606*(3), 85.

Danielson, J. J., & Gesch, D. B. (2011). *Global multi-resolution terrain elevation data 2010 (GMTED2010)*. U.S. Geological Survey Open-File Report, 2011-1073.

Dee, D. P., Uppala, S. M., Simmons, A. J., Berrisford, P., Poil, P., Kobayashi, S., et al. (2011). The ERA-Interim reanalysis: Configuration and performance of the data assimilation system. *Quarterly Journal of the Royal Meteorological Society*, *137*, 553–597. https://doi.org/10.1002/qj.828

Densmore, C. R., Sanabia, E. R., & Barrett, B. S. (2019). QBO influence on MJO amplitude over the Maritime Continent: Physical mechanisms and seasonality. *Monthly Weather Review*, *147*, 389–406. https://doi.org/10.1175/MWR-D-18-0158.1

Ebert, E. E., Janowiak, J. E., & Kidd, C. (2007). Comparison of near-real-time precipitation estimates from satellite observations and numerical models. *Bulletin of the American Meteorological Society*, *88*, 47–64. https://doi.org/10.1175/BAMS-88-1-47

Feng, J., Li, T., & Zhu, W. (2015). Propagating and nonpropagating MJO events over Maritime Continent. *Journal of Climate*, *28*, 8430–8449. https://doi.org/10.1175/JCLI-D-15-0085.1

Flatau, M., Flatau, P. J., Phoebus, P., & Niller, P. P. (1997). The feedback between equatorial convection and local radiative and evaporative processes: The implications for intraseasonal oscillation. *Journal of the Atmospheric Science*, *54*, 2373–2386. https://doi.org/10.1175/1520-0469(1997)054<2373:TFBECA>2.0.CO;2

Gianotti, R. L., Zhang, D., & Eltahir, E. A. B. (2012). Assessment of the Regional Climate Model version 3 over the Maritime Continent using different cumulus parameterization and land surface schemes. *Journal of Climate*, *25*, 638–656. https://doi.org/10.1175/JCLI-D-11-00025.1

Gill, A. E. (1980). Some simple solutions for heat-induced tropical circulation. *Quarterly Journal of the Royal Meteorological Society*, *106*, 447–462.

Hagos, S., & Leung, L. R. (2011). Moist thermodynamics of the Madden–Julian oscillation in a cloud-resolving simulation. *Journal of Climate*, *24*, 5571–5583. https://doi.org/10.1175/2011JCLI4212.1

Hagos, S. M., Zhang, C., Feng, Z., Burleyson, C. D., De Mott, C., Kerns, B., et al. (2016). The impact of the diurnal cycle on the propagation of Madden–Julian Oscillation convection across the Maritime Continent. *Journal of Advances in Modeling Earth System*, *8*, 1552–1564. https://doi.org/10.1002/2016MS000725

Hassim, M. E. E., Lane, T. P., & Grabowski, W. W. (2016). The diurnal cycle of rainfall over New Guinea in convection permitting WRF simulations. *Atmosphere Chemistry Physics*, *16*, 161–175. https://doi.org/10.5194/acp-16-161-2016

Hersbach, H., Bell, B., Berrisford, P., Hirahara, S., Horányi, A., Muñoz-Sabater, J., et al. (2020). The ERA5 global reanalysis. *Quarterly Journal of the Royal Meteorological Society*, *146*, 1999–2049. https://doi.org/10.1002/qj.3803

Holloway, C. E., Woolnough, S. J., & Lister, G. M. S. (2013). The effects of explicit versus parameterized convection on the MJO in a Large-domain high-resolution tropical case study. Part I: Characterization of large-scale organization and propagation. *Journal of the Atmospheric Science*, *70*, 1342–1369. https://doi.org/10.1175/JAS-D-12-0227.1

Hsu, H. H., & Lee, M. Y. (2005). Topographic effects on the eastward propagation and initiation of the Madden–Julian oscillation. *Journal of Climate*, *18*, 795–809. https://doi.org/10.1175/JCLI-3292.1

Hsu, P. C., & Li, T. (2012). Role of the boundary layer moisture asymmetry in causing the eastward propagation of the Madden–Julian Oscillation. *Journal of Climate*, *25*, 4914–4931. https://doi.org/10.1175/JCLI-D-11-00310.1

Huffman, G. J., Bolvin, D. T., Nelkin, E. J., Wolff, D. B., Adler, R. F., Gu, G., et al. (2007). The TRMM Multisatellite Precipitation Analysis (TMPA): Quasi-global, multiyear, combined-sensor precipitation estimates at fine scales. *Journal of Hydrometeorology*, *8*, 38–55. https://doi.org/10.1175/JHM560.1

Hung, M. P., Lin, J. L., Wang, W., Kim, D., Shinoda, T., & Weaver, S. J. (2013). MJO and convectively coupled equatorial waves simulated by CMIP5 climate models. *Journal of Climate*, *26*, 6185–6214. https://doi.org/10.1175/JCLI-D-12-00541.1

Iacono, M. J., Delamere, J. S., Mlawer, E. J., Shephard, M. W., Clough, S. A., & Collins, W. D. (2008). Radiative forcing by long–lived greenhouse gases: Calculations with the AER radiative transfer models. *Journal of Geophysical Research Atmosphere*, *113*(D13103), https://doi.org/10.1029/2008JD009944

Im, E. S., & Elthair, E. (2018). Simulation of the diurnal variation of rainfall over the western Maritime Continent using a regional climate model. *Climate Dynamics*, *51*, 73–88. https://doi.org/10.1007/s00382-017-3907-3

Inness, P. M., & Slingo, J. M. (2006). The interaction of the Madden–Julian oscillation with the maritime continent in a GCM. *Quarterly Journal of the Royal Meteorological Society*, *132*, 1645–1667. https://doi.org/10.1256/qj.05.102

Iskandar, I. (2010). Seasonal and interannual patterns of sea surface temperature in Banda Sea as revealed by self-organizing map. *Continental Shelf Research*, *30*(9), 1136–1148. https://doi.org/10.1016/j.csr.2010.03.003

Janjic, Z. I. (1994). The step-mountain Eta coordinate model: further developments of the convection, viscous sublayer and turbulence closure schemes. *Monthly Weather Review*, *122*, 927–945.

Jiang, X., Su, H., & Waliser, D. E. (2019). A damping effect of the Maritime Continent for the Madden–Julian Oscillation. *Journal of Geophysical Research: Atmospheres*, *124*, 693–13713. https://doi.org/10.1029/2019JD031503

Joyce, J., & Xie, P. (2011). Kalman filter-based CMORPH. *Journal of Hydrometeorology*, *12*, 1547–1563. https://doi.org/10.1175/JHM-D-11-022.1

Kain, J. S. (2004). The Kain–Fritsch convective parameterization: An update. *Journal of Applied Meteorology and Climatology*, *43*, 170–181. https://doi.org/10.1175/1520-0450(2004)043<0170:TKCPAU>2.0.CO;2

Kanamori, H., Yasunari, T., & Kuraji, K. (2012). Modulation of the diurnal cycle of rainfall associated with the MJO observed by a dense hourly rain gauge network at Sarawak, Borneo. *Journal of Climate*, *24*, 4858–4875. https://doi.org/10.1175/JCLI-D-12-00158.1

Kerns, B. W., & Chen, S. Y. (2020). A 20-year climatology of Madden–Julian oscillation convection: Large-scale precipitation tracking from TRMM-GPM Rainfall. *Journal of Geophysical Research: Atmospheres*, *125*, e2019JD032142. https://doi.org/10.1029/2019JD032142

Kida, S., & Richards, K. J. (2009). Seasonal sea surface temperature variability in the Indonesian Seas. *Journal of Geophysical Research*, *114*, C06016. https://doi.org/10.1029/2008JC005150

Kikuchi, K., & Wang, B. (2008). Diurnal precipitation regimes in the global tropics. *Journal of Climate*, *21*, 2680–2696. https://doi.org/10.1175/2007JCLI2051.1

Kiladis, G. N., Dias, J., Straub, K. H., Wheeler, M. C., Tulich, S. N., Kikuchi, K., et al. (2014). A comparison of OLR and circulation based indices for tracking the MJO. *Monthly Weather Review*, *142*, 1697–1715. https://doi.org/10.1175/MWR-D-13-00301.1

Kim, D., Kug, J. S., & Sobel, A. H. (2014). Propagating versus nonpropagating Madden–Julian oscillation events. *Journal of Climate*, *27*, 111–125. https://doi.org/10.1175/JCLI-D-13-00084.1

Kwan, M. S., Tangang, F. T., & Juneng, L. (2013). Present-day regional climate simulation over Malaysia and western Maritime Continent region using PRECIS forced with ERA40 reanalysis. *Theoretical and Applied Climatology*, *115*, 1–14. https://doi.org/10.1007/s00704-013-0873-5

LaFleur, D. M., Barrett, B. S., & Henderson, G. R. (2015). Some climatological aspects of the Madden–Julian Oscillation (MJO). *Journal of Climate*, *28*, 6039–6053. https://doi.org/10.1175/JCLI-D-14-00744.1

Lau, K.-M., & Peng, L. (1987). Origin of low-frequency (intraseasonal) oscillations in the tropical atmosphere. Part I: Basic theory. *Journal of the Atmosphere Science*, *44*, 950–972.

Leutwyler, D., Lüthi, D., Ban, N., Fuhrer, O., & Schär, C. (2017). Evaluation of the convection-resolving climate modeling approach on continental scales. *Journal of Geophysical Research: Atmospheres*, *122*, 5237–5258. https://doi.org/10.1002/2016JD026013

Lim, K. S. S, & Hong, S. Y. (2010). Development of an effective double-moment cloud microphysics scheme with prognostic cloud condensation nuclei (CCN) for weather and climate models. *Monthly Weather Review*, *138*, 1587–1612. https://doi.org/10.1175/2009MWR2968.1

Lin, J.-L., Kiladis, G. N., Mapes, B. E., Weickmann, K. M., Sperber, K. R., Lin, W., et al. (2006). Tropical intraseasonal variability in 14 IPCC AR4 climate models. Part I: Convective signals. *Journal of Climate*, *19*, 2665–2690. https://doi.org/10.1175/JCLI3735.1

Love, B., Matthews, A. J., & Lister, G. M. S. (2011). The diurnal cycle of precipitation over the Maritime Continent in a high-resolution atmospheric model. *Quarterly Journal of the Royal Meteorological Society*, *137*, 934–947. https://doi.org/10.1002/qj.809

Lu, J. H., & Wang, L. (2019). Precipitation diurnal cycle over the Maritime Continent modulated by the MJO. *Climate Dynamics*, *53*, 6489–6501. https://doi.org/10.1007/s00382-019-04941-8

Madden, R. A., & Julian, P. R. (1971). Detection of a 40–50 day oscillation in the zonal wind of the tropical pacific. *Journal of the Atmosphere Science*, *28*, 702–708.

Madden, R. A., & Julian, P. R. (1972). Description of global-scale circulation cells in the tropics with a 40–50 day period. *Journal of the Atmosphere Science*, *29*, 1109–1123.

Matsuno, T. (1966). Quasi-geostrophic motions in the equatorial area. *Journal of the Meteorological Society of Japan*, *44*, 25–42.

Matthews, A. J. (2008). Primary and successive events in the Madden–Julian oscillation. *Quarterly Journal of the Royal Meteorological Society*, *134*, 439–453. https://doi.org/10.1002/qj.224

Moncrieff, M. W. (2019). Toward a dynamical foundation for organized convection parameterization in GCMs. *Geophysical Research Letter*, *46*, 14103–14108. https://doi.org/10.1029/2019GL085316

Moncrieff, M. W., Waliser, D. E., & Caugley, J. (2012). Progress and direction in tropical convection research: YOTC international science symposium. *Bulletin of the American Meteorological Society*, *93*, ES65–ES69. https://doi.org/10.1175/BAMS-D-11-00253.1

Moncrieff, M. W., Waliser, D. E., Miller, M. J., Shapiro, M. A., Asrar, G. R., & Caugley, J. (2012). Multiscale convective organization and the YOTC virtual global field campaign. *Bulletin of the American Meteorological Society*, *93*, 1171–1187. https://doi.org/10.1175/BAMS-D-11-002333.1

Moum, J. N., Szoeke, S. P., Smyth, W. D., Edson, J. B., DeWitt, H. L., Moulin, A. J., et al. (2014). Air–sea interactions from westerly wind bursts during the November 2011 MJO in the Indian Ocean. *Bulletin of the American Meteorological Society*, 1185–1199. https://doi.org/10.1175/BAMS-D-12-00225.1

Oh, J. H., Kim, K. Y., & Lim, G. H. (2012). Impact of MJO on the diurnal cycle of rainfall over the western Maritime Continent in the austral summer. *Climate Dynamics*, *38*, 1167–1180. https://doi.org/10.1007/s00382-011-1237-4

Peatman, S. C., Matthews, A. J., & Stevens, D. P. (2014). Propagation of the Madden–Julian Oscillation through the Maritime Continent and scale interaction with the diurnal cycle of precipitation. *Quarterly Journal of the Royal Meteorological Society*, *140*, 814–825. https://doi.org/10.1002/qj.2161

Platnick, S., Hubanks, P., Meyer, K., & King, M. D. (2015). *MODIS Atmosphere L3 Monthly Product (08_L3). NASA MODIS Adaptive Processing System*. Goddard Space Flight Center.

Qian, J.-H. (2007). Why precipitation is mostly concentrated over islands in the Maritime Continent. *Journal of the Atmosphere Science*, *65*, 1428–1441. https://doi.org/10.1175/2007JAS2422.1

Qian, J.-H. (2019). Mechanisms for the dipolar patterns of rainfall variability over large islands in the Maritime Continent associated with the Madden–Julian Oscillation. *Journal of the Atmosphere Science*, *77*, 2257–2278. https://doi.org/10.1175/JAS-D-19-0091.1

Rachman, H. A., Gaol, J. L., Syamsudin, F., & As-syakur, A. (2020). Influence of coastal upwelling on sea surface temperature trends Banda Sea. *IOP Conference Series: Earth and Environmental Science*, *429*, 012015. https://doi.org/10.1088/1755-1315/429/1/012015

Ramage, C. S. (1968). Role of a tropical "Maritime Continent" in the atmospheric circulation. *Monthly Weather Review*, *96*, 365–379.

Rauniyar, S. P., & Walsh, K. J. (2011). Scale interaction of the diurnal cycle of rainfall over the Maritime Continent and Australia: Influence of the MJO. *Journal of Climate*, *24*, 325–348. https://doi.org/10.1175/2010JCLI3673.1

Rauniyar, S. P., & Walsh, K. J. E. (2013). Influence of ENSO on the diurnal cycle of rainfall over the Maritime Continent and Australia. *Journal of Climate*, *26*, 1304–1321. https://doi.org/10.1175/JCLI-D-12-00124.1

Ray, P., & Li, T. (2013). Relative roles of circumnavigating waves and extratropics on the MJO and its relationship with the mean state. *Journal of the Atmosphere Science*, *70*, 876–893. https://doi.org/10.1175/JAS-D-12-0153.1

Ray, P., Zhang, C., Dudhia, J., & Chen, S. S. (2009). A numerical case study on the initiation of the Madden–Julian oscillation. *Journal of the Atmospheric Science*, *66*, 310–331. https://doi.org/10.1175/2008JAS2701.1

Ray, P., Zhang, C., Dudhia, J., Li, T., & Moncrieff, M. W. (2012). Tropical channel model. In L. M. Druyan (Ed.), *Climate models* (pp. 3–18). InTech Open Access Publisher.

Ray, P., Zhang, C., Moncrieff, M. W., Dudhia, J., Caron, J. M., Leung, R., & Bruyere, C. (2011). Role of the atmospheric mean state on the initiation of the Madden–Julian Oscillation in a tropical channel Model. *Climate Dynamics*, *36*, 161–184. https://doi.org/10.1007/s00382-010-0859-2

Riley Dellaripa, E. M., Maloney, E. D., Toms, B. A., Saleeby, S. M., & van den Heever, S. C. (2019). Topographic effects on the Luzon diurnal cycle during the BSISO. *Journal of the Atmospheric Science*, *77*, 3–30. https://doi.org/10.1175/JAS-D-19-0046.1

Rui, H., & Wang, B. (1990). Development characteristics and dynamics structure of tropical intraseasonal convection anomalies. *Journal of the Atmospheric Sciences*, *47*, 357–379.

Ruppert, J. H., Jr., & Chen, X. (2020). Island rainfall enhancement in the Maritime Continent. *Geophysical Research Letters*, *47*, e2019GL086545. https://doi.org/10.1029/2019GL086545

Ruppert, J. H., Jr., Chen, X., & Zhang, F. (2020). Convectively forced diurnal gravity waves in the Maritime Continent. *Journal of the Atmospheric Science*, *77*, 1119–1136. https://doi.org/10.1175/JAS-D-19-0236.1

Ruppert, J. H., Jr., & Zhang, F. (2019). Diurnal forcing and phase locking of gravity waves in the Maritime Continent. *Journal of the Atmospheric Sciences*, *76*, 2815–2835. https://doi.org/10.1175/JAS-D-19-0061.1

Sarr, A.-C., Sepulchre, P., & Husson, L. (2019). Impact of the Sunda shelf on the climate of the Maritime Continent. *Journal of Geophysical Research: Atmospheres*, *124*, 2574–2588. https://doi.org/10.1029/2018JD029971

Seo, K.-H., & Kim, K.-Y. (2003). Propagation and initiation mechanisms of the Madden–Julian oscillation. *Journal of Geophysical Research*, *108*(D13), 4384. https://doi.org/10.1029/2002JD002876

Shi, J. J., Tao, W. K., Matsui, T, Cifelli, R., Hou, A., & Lang, S. (2010). WRF simulations of the 20–22 January 2007 snow events over eastern Canada: comparison with in situ and satellite observations. *Journal of Applied Meteororlogy*, *49*, 2246–2266. https://doi.org/10.1175/2010JAMC2282.1

Simpson, J., Keenan, T. D., Ferrier, B., Simpson, R. H., & Holland, G. J. (1993). Cumulus merger in the Maritime Continent region. *Meteorology and Atmospheric Physics*, *51*, 73–99. https://doi.org/10.1007/BF01080881

Skamarock, W. C., Klemp, J. B., Dudhia, J., Gill, D. O., Barker, D., Duda, M. G., et al. (2008). *A description of the advanced research WRF version 3, NCAR Tech, Note NCAR/TN-475 + STR* (p. 125). Boulder, CO: National Center for Atmospheric Research.

Skok, G., Zagar, N., Honzak, L., Zabkar, R., Rakovec, J., & Ceglar, A. (2016). Precipitation intercomparison of a set of satellite- and raingauge-derived datasets, ERA Interim reanalysis, and a single WRF regional climate simulation over Europe and the North Atlantic. *Theoretical and Applied Climatology*, *123*, 217–232. https://doi.org/10.1007/s00704-014-1350-5

Sobel, A. H., Maloney, E. D., Bellon, G., & Frierson, D. M. (2010). Surface fluxes and tropical intraseasonal variability: A reassessment. *Journal of Advances in Modeling Earth System*, *2*, 2. https://doi.org/10.3894/JAMES.2010.2.2

Sui, C.-H., & Lau, K. M. (1992). Multiple phenomena in the tropical atmosphere over the western Pacific, *Monthly Weather Review*, *120*, 407–430.

Sui, C.-H., Li, X., Lau, K.-M., & Adamec, D. (1997). Multiscale air–sea interactions during TOGA COARE. *Monthly Weather Review*, *125*, 448–462.

Suzuki, T. (2009). Diurnal cycle of deep convection in super clusters embedded in the Madden–Julian Oscillation. *Journal of Geophysical Research*, *114*, D22102. https://doi.org/10.1029/2008JD011303

Tan, H., Ray, P., Barrett, B. S., Tewari, M., & Moncrieff, M. W. (2020). Role of topography on the MJO in the maritime continent: A numerical case study. *Climate Dynamics*, *55*, 295–314. https://doi.org/10.1007/s00382-018-4275-3

Tian, B. J., Waliser, D. E., & Fetzer, E. J. (2006). Modulation of the diurnal cycle of tropical deep convective clouds by the MJO. *Geophysical Research Letters*, *33*, L20704. https://doi.org/10.1029/2006GL027752

Tseng, W. L., Hsu, H. H., Keenluside, N., Chang, C. W. J., Tsuang, B. J., Tu, C. Y., & Jiang, L. C. (2017). Effects of surface orography and land–sea contrast on the Madden–Julian Oscillation in the Maritime Continent: A numerical study using ECHAM5-SIT. *Journal of Climate*, *30*, 9725–9741. https://doi.org/10.1175/JCLI-D-17-0051.1

Tseng, W. L., Tsuang, B. J., Keenlyside, N., Hsu, H. H., & Tu, C. Y. (2015). Resolving the upper-ocean warm layer improves the simulation of the Madden–Julian oscillation. *Climate Dynamics*, *44*, 1487–1503. https://doi.org/10.1007/s00382-014-2315-1

Vincent, C. L., & Lane, T. P. (2016). Evolution of the diurnal precipitation cycle with the passage of a Madden–Julian Oscillation event through the Maritime Continent. *Monthly Weather Review*, *144*, 1983–2005. https://doi.org/10.1175/MWR-D-15-0326.1

Waliser, D. E., Moncrieff, M. W., Burridge, D., Fink, A. H., Gochis, D., Goswami, B. N., et al. (2012). The "year" of tropical convection (May 2008 to April 2010): Climate variability and weather highlights. *Bulletin of the American Meteorological Society*, *93*, 1189–1218. https://doi.org/10.1175/2011BAMS3095.1

Wang, S., & Sobel, A. H. (2017). Factors controlling rain on small tropical islands: Diurnal cycle, large-scale wind speed, and topography. *Journal of the Atmospheric Sciences*, *74*, 3515–3532. https://doi.org/10.1175/JAS-D-16-0344.1

Wang, S., Sobel, A. H., Zhang, F., Sun, Y. Q., Yue, Y., & Zhou, L. (2015). Regional simulation of the October and November MJO events observed during the CINDY/DYNAMO field campaign at gray zone resolution. *Journal of Climate*, *28*, 2097–2119. https://doi.org/10.1175/JCLI-D-14-00294.1

Wei, Y., Pu, Z., & Zhang, C. (2020). Diurnal cycle of precipitation over the Maritime Continent under modulation of MJO: Perspectives from cloud-permitting scale simulations. *Journal of Geophysical Research: Atmospheres*, *125*, e2020JD032529. https://doi.org/10.1029/2020JD032529

Wheeler, M. C., & Hendon, H. H. (2004). An all-season real-time multivariate MJO index: Development of an index for monitoring and prediction. *Monthly Weather Review*, *132*(8), 1917–1932. https://doi.org/10.1175/1520-0493(2004)132<1917:AARMMI>2.0.CO;2

Wu, C. H., & Hsu, H. H. (2009). Topographic influence on the MJO in the Maritime Continent. *Journal of Climate*, *22*, 5433–5448. https://doi.org/10.1175/2009JCLI2825.1

Yang, G.-Y., & Slingo, J. (2001). The diurnal cycle in the Tropics. *Monthly Weather Review*, *129*, 784–801. https://doi.org/10.1175/1520-0493(2001)129<0784:TDCITT>2.0.CO;2

Yilmaz, K. K., HogueHsu, T. S. K. L., Sorooshian, S., Gupta, H. V., & Wagener, T. (2005). Intercomparison of rain gauge, radar, and satellite-based precipitation estimates with emphasis on hydrologic forecasting. *Journal of Hydrometeorology*, *6*, 497–517. https://doi.org/10.1175/JHM431.1

Zhang, C. (2005). Madden–Julian Oscillation. *Review of Geophysics*, *43*, RG2003. https://doi.org/10.1029/2004RG000158

Zhang, C., & Dong, M. (2004). Seasonality in the Madden–Julian Oscillation. *Journal of Climate*, *17*, 3169–3180. https://doi.org/10.1175/1520-0442(2004)017<3169:SITMO>2.0.CO;2

Zhang, C., & Ling, J. (2017). Barrier effect of the Indo-Pacific Maritime Continent on the MJO: Perspectives from tracking MJO precipitation. *Journal of Climate*, *30*, 3439–3459. https://doi.org/10.1175/JCLI-D-16-0614.1

Zhou, X., Ray, P., Barrett, B. S., & Hsu, P.-C. (2020). Understanding the bias in surface latent and sensible heat fluxes in contemporary AGCMS over tropical oceans. *Climate Dynamics*, *55*, 2957–2978. https://doi.org/10.1007/s00382-020-05431-y